ELECTRONIC SUPPORTING INFORMATION

Record efficiency of 1000 nm electroluminescence from the solution-processable host-free OLED

Anton D. Kovalenko [a], Lyubov O. Tcelykh [a], Daniil Koshelev [a], Andrey A. Vashchenko[b], Dmitry M. Tsymbarenko[a], Alexander S. Goloveshkin[c], Aleksey Aleksandrov [d], Anatolii Burlov [e], Valentina V. Utochnikova* [a]

a. M.V. Lomonosov Moscow State University, 1/3 Leninskye Gory, Moscow 119991, Russia

b. P.N. Lebedev Physical Institute, Leninsky prosp. 53 Moscow 119992, Russia

c. A.N.Nesmeyanov Institute of Organoelement Compounds RAS, Vavilova 28, Moscow, Russia, 119991

d. Frumkin Institute of Physical Chemistry and Electrochemistry RAS, Leninskiy prosp., 31, Moscow, 119071

e. Institute of Physical & Organic Chemistry, Southern Federal University, Stachka Avenue, 194/2, 344090 Rostov-on-Don, Russia

Contents

Experimental

Synthesis of the organic ligands

Ligands H_2L^1 and H_2L^2 and complexes Ln(L)(HL) (L = **L^1, L^2**) were synthesized according to the previously reported procedure[1]. Ln(L)(HL) (Ln = Eu, Gd, Yb, Lu**;** L = **L^1, L^2**) were obtained from freshly prepared $Ln(OH)_3$ and H_2L^1.

$K(H_2O)_2(EtOH)[Yb(L^2)_2]$ and $K(H_2O)_2[Yb(L^1)_2]$ were obtained dissolving corresponding $Yb(L^n)(HL^n)$ (n = 1, 2) in ethanolic KOH (reaction (2)) by the following procedure: 0.10 mmol of Ln(L)(HL) were dispersed in 50 ml of boiling ethanol under stirring. 0.090 mmol of KOH was added, the mixture was stirred for 15 min, hot-filtered, and cooled down to room temperature. During the evaporation of the solution, a crystalline precipitate was obtained, which was filtered, washed with ethanol, and dried.

Single crystals of $K(C_2H_5OH)_2[Yb(L^2)_2]$ and $K(THF)_2[Yb(L^1)_2]$ were grown from EtOH and THF respectively. A suitable crystal was selected and mounted on a glass needle on a Bruker APEX-II CCD diffractometer. The crystal was kept at 120 K during data collection. Using Olex2 [2], the structure was solved with the XS [2] structure solution program using Direct Methods and refined with the XL[3] refinement package using Least Squares minimization.

Crystal structure determination of $K(C_2H_5OH)_2[Yb(L^2)_2]$

Crystal Data for $C_{56}H_{56}KN_6O_9S_2Yb$ (M =1233.32 g/mol): monoclinic, space group $P2_1/n$ (no. 14), a = 9.104(2) Å, b = 27.169(7) Å, c = 23.237(6) Å, β = 90.797(5)°, V = 5747(3) Å^3, Z = 4, T = 120 K, μ(MoKα) = 1.831 mm^{-1}, *Dcalc* = 1.425 g/cm^3, 11908 reflections measured (1.498° ≤ 2Θ ≤ 48.812°), 9459 unique (R_{int} = 0.0466, R_{sigma} = 0.0504) which were used in all calculations. The final R_1 was 0.0816 (I > 2σ(I)) and wR_2 was 0.2165 (all data).

Crystal structure determination of $K(THF)_2[Yb(L^1)_2]$

Crystal Data for $C_{50}H_{50}KN_6O_8S_2Yb$ (M =1139.22 g/mol): monoclinic, space group $P2_1/n$ (no. 14), a = 15.3880(7) Å, b = 17.1596(8) Å, c = 18.1761(9) Å, β = 94.562(2)°, V = 4784.2(4) Å^3, Z = 4, T = 120 K, μ(MoKα) = 2.190 mm^{-1}, *Dcalc* = 1.582 g/cm^3, 62887 reflections

measured ($3.268° \leq 2\Theta \leq 61.074°$), 14587 unique ($R_{int} = 0.0842$, $R_{sigma} = 0.1058$) which were used in all calculations. The final R_1 was 0.0461 ($I > 2\sigma(I)$) and wR_2 was 0.1126 (all data).

Photoluminescence spectra in the visible range were recorded on a Fluoromax spectrometer. Photoluminescence spectra at 77 K were recorded on the same device by placing the sample in the liquid nitrogen cryostat.

Photoluminescence spectra in the NIR range were measured using the OceanOptics Maya2000 Spectrometer under the excitation with the xenon lamp from the Fluoromax spectrometer.

Quantum yields in the NIR range were determined using the same equipment supplied with the PTI K-sphere-petite integrating sphere from Horiba Tobin Yvon (3.2") using the absolute method, pregraduated in the range of 200-1100 nm using electric measuring wide-range incandescent lamp of SIRSH type. Samples were excited at 400 nm

Diffuse reflection spectra were recorded using a PerkinElmer LAMBDA 950 spectrometer.

Thermal analysis was carried out on a thermoanalyzer STA 409 PC Luxx (NETZSCH, Germany) in the temperature range of 20-1000 ºC in air, heating rate 10 º/min. *IR spectra* in the ATR mode were recorded on a spectrometer Spectrum One (Perkin-Elmer) in the region of 400-4000 cm^{-1}. *X-ray powder diffraction* (XRD) measurements were performed on a Bruker D8 Advance diffractometer (Vario geometry) in the 2θ range of 4–80° equipped with a Cu Kα1 Ge(111) focusing monochromator and a LynxEye onedimensional position-sensitive detector. The powder X-ray diffraction patterns were indexed using TOPAS 5.0 software. ***Absorption spectra*** were obtained using Perkin Elmer LAMBDA 950 spectrometer.

OLED manufacturing

Substrate preparation. Substrates with pre-patterned ITO of 12 Ohm/sq resistance were purchased from Lumtec Taiwan. Before spin-coating, the substrates underwent a standard cleaning procedure of ultrasonication in KOH solution, bidistillated water, isopropanol for 15 minutes each followed by drying with nitrogen flow. Then the substrates were placed in a UV-

cleaning chamber (Ossila UK) where additional cleaning and O_3 – enrichment of ITO took place for 25 minutes to increase the wettability of the substrates.

Solutions spin-coating. We used a spin coater KW-4A by Chemat Technology operating in the air. **The thermal deposition** was performed in a vacuum less than 10^{-3} Pa from a quartz cuvette heated by tantalum spiral. The obtained devices were encapsulated with Star Technology UV-curable adhesive UVA-4103. The deposition rate was measured in situ by a deposition controller Leybold Inficon IC-6000 calibrated by NT-MDT atomic force microscope of Integra family. Thicknesses of spin-coated films were also measured by NT-MDT atomic force microscope directly on OLED structures.

Deposition parameters:

PEDOT-PSS	Spin-coating at 2000rpm, thermal treatment at 130C for 20 min, 50 nm
poly-TPD	Spin-coating at 2000rpm, thermal treatment at 100C for 10 min, 15 nm
PVK	Spin-coating at 2000rpm, thermal treatment at 100C for 10 min, 15 nm
$KYb(L^1)_2$	Spin-coating at 1000rpm, thermal treatment at 120C for 30 min, 31 nm
$KYb(L^2)_2$	Spin-coating at 1000rpm, thermal treatment at 120C for 30 min, 23 nm
TPBi	VTE, 13 nm
OXD-7	VTE, 13 nm

The electroluminescence spectra were obtained with an Ocean Optics Maya 2000 Pro CCD spectrometer sensitive within 200-1100 nm. Current-voltage characteristics were obtained using two DT 838 Digital multimeters. OLED optical power was determined using a Coherent FieldMaxII Laser Power Meter with an optic filter removing the visible part of the spectra.

XRD data

Table S1. Lattice parameters of $Eu(L^2)(HL^2)$ and $Yb(L^2)(HL^2)$

Complex	**$Eu(L^2)(HL^2)$**	**$Yb(L^2)(HL^2)$**	**$K(C_2H_5OH)_2[Yb(L^2)_2]$**	**$K(THF)_2[Yb(L^1)_2]$**
Space-group	$P2_1/c$	$P2_1/c$	$P2_1/n$	$P2_1/n$
Cell Volume ($Å^3$)	9943	9140	5747(2)	4784(2)
a (Å)	21.830(14)	15.55(2)	9.104(2)	15.388(7)
b (Å)	30.72(3)	26.41(3)	27.169(7)	17.160(8)
c (Å)	22.139(14)	22.67(3)	23.237(6)	18.176(9)
beta (°)	137.96(5)	101.17(8)	90.797(5)	94.56(2)

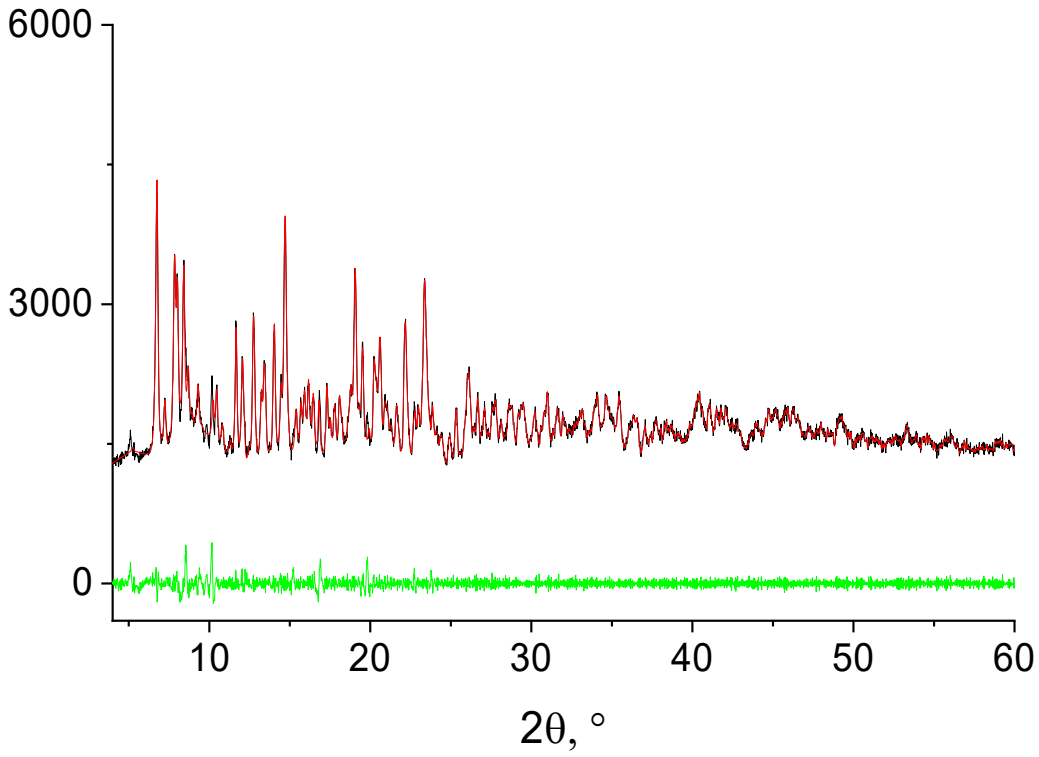

Fig. S 1 XRD pattern of Eu(L^2)(HL^2) powder: experimental (black), fit (red), difference (green)

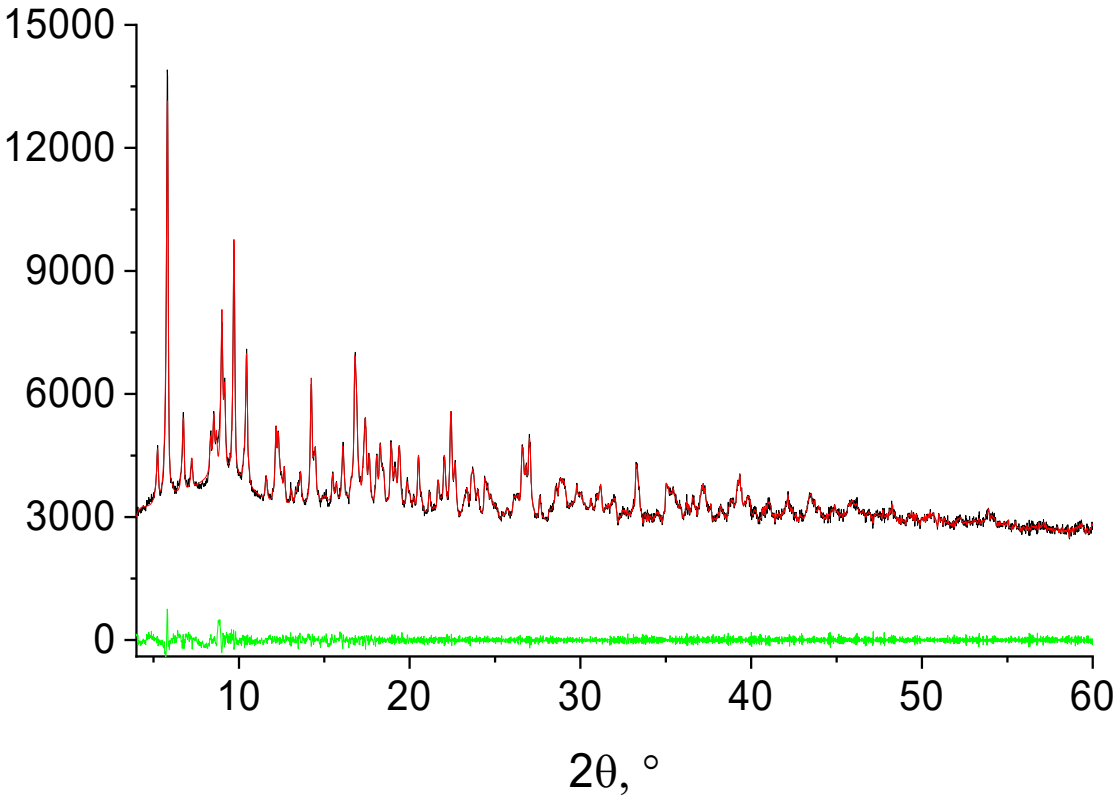

Fig. S 2 XRD pattern of Gd(L^2)(HL^2) powder: experimental (black), fit (red), difference (green)

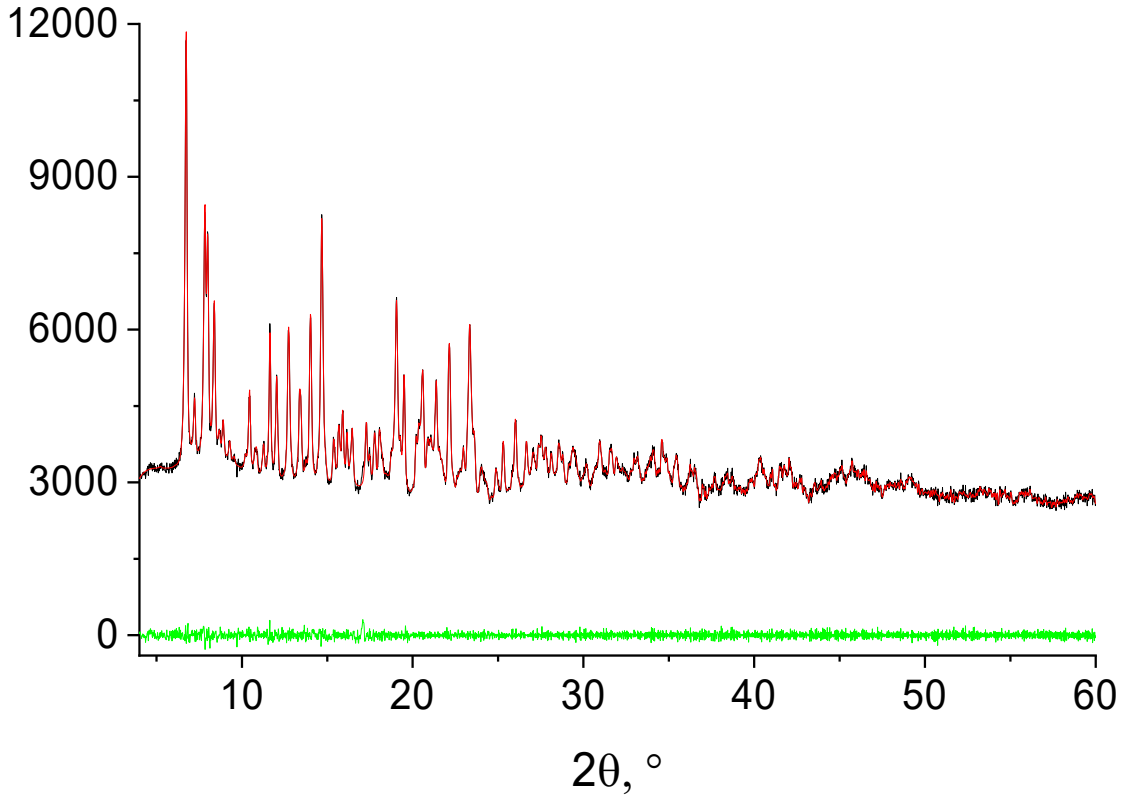

Fig. S 3 XRD pattern of Yb(L^2)(HL^2) powder: experimental (black), fit (red), difference (green)

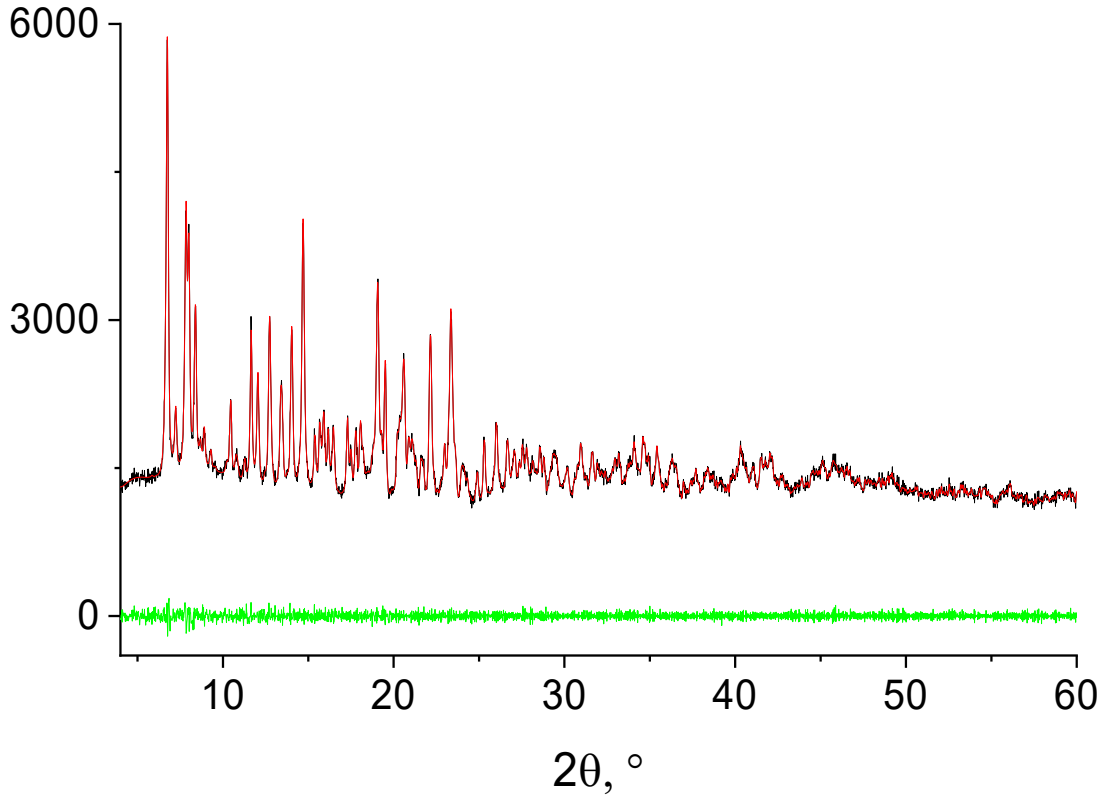

Fig. S 4 XRD pattern of Lu(L^2)(HL^2) powder: experimental (black), fit (red), difference (green)

IR spectroscopy

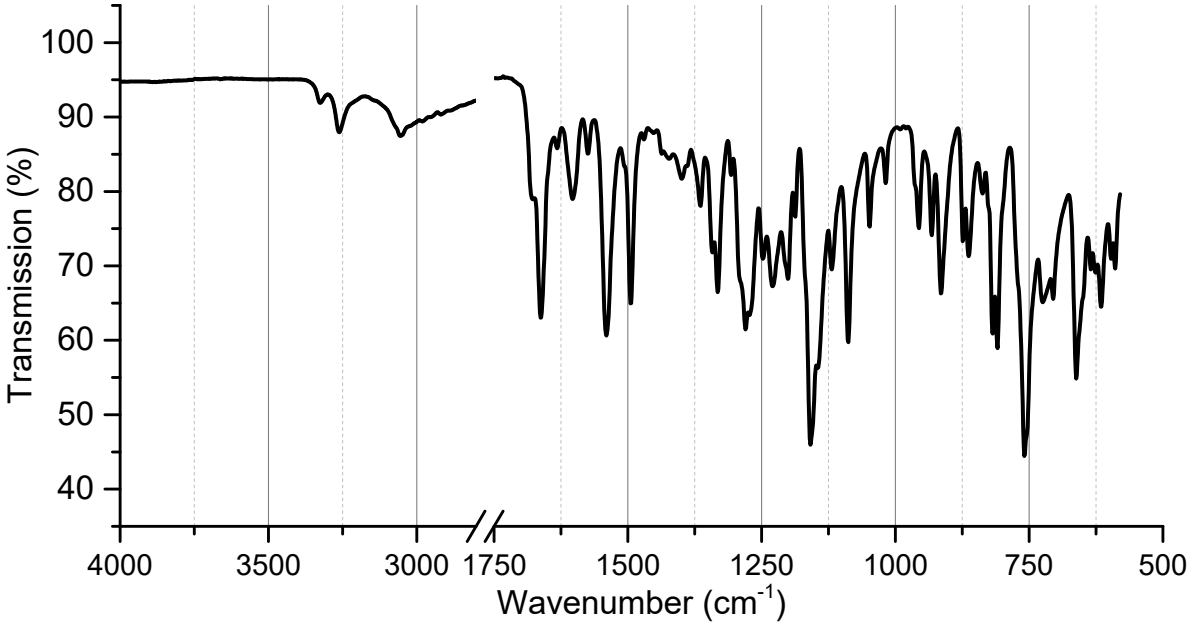

Fig. S 5 IR spectrum of H_2L^2

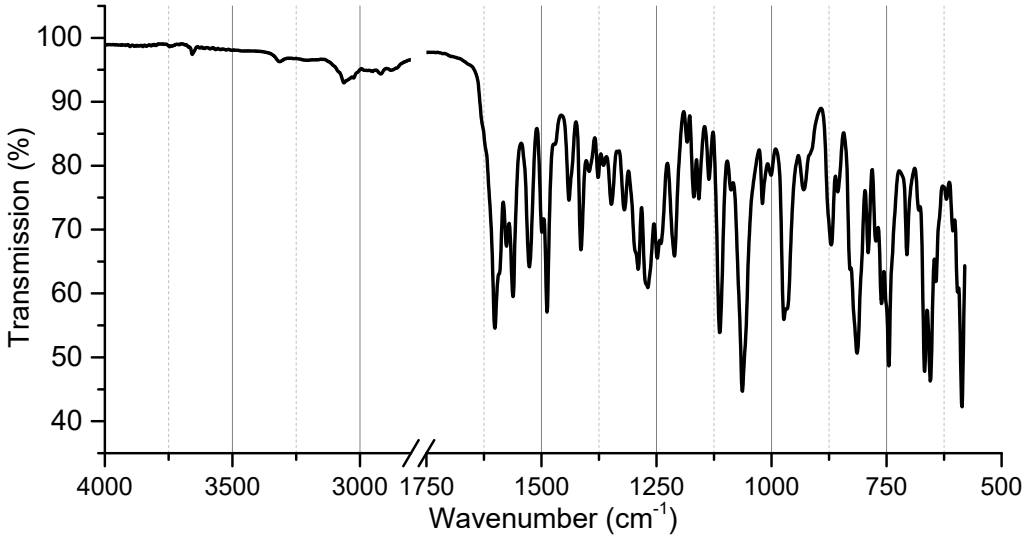

Fig. S 6 IR spectrum of $Yb(L^2)(HL^2)$

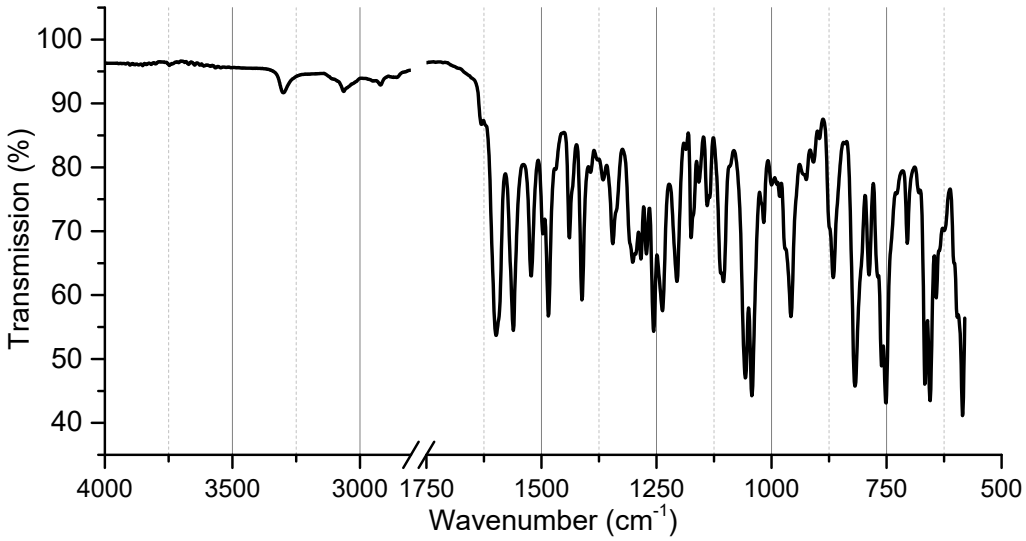

Fig. S 7 IR spectrum of $Gd(L^2)(HL^2)$

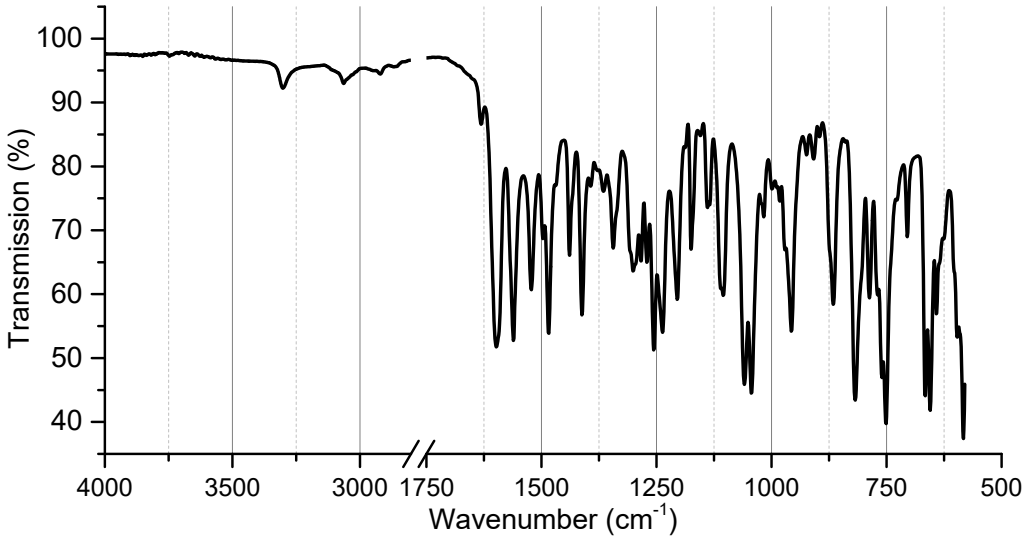

Fig. S 8 IR spectrum of $Eu(L^2)(HL^2)$

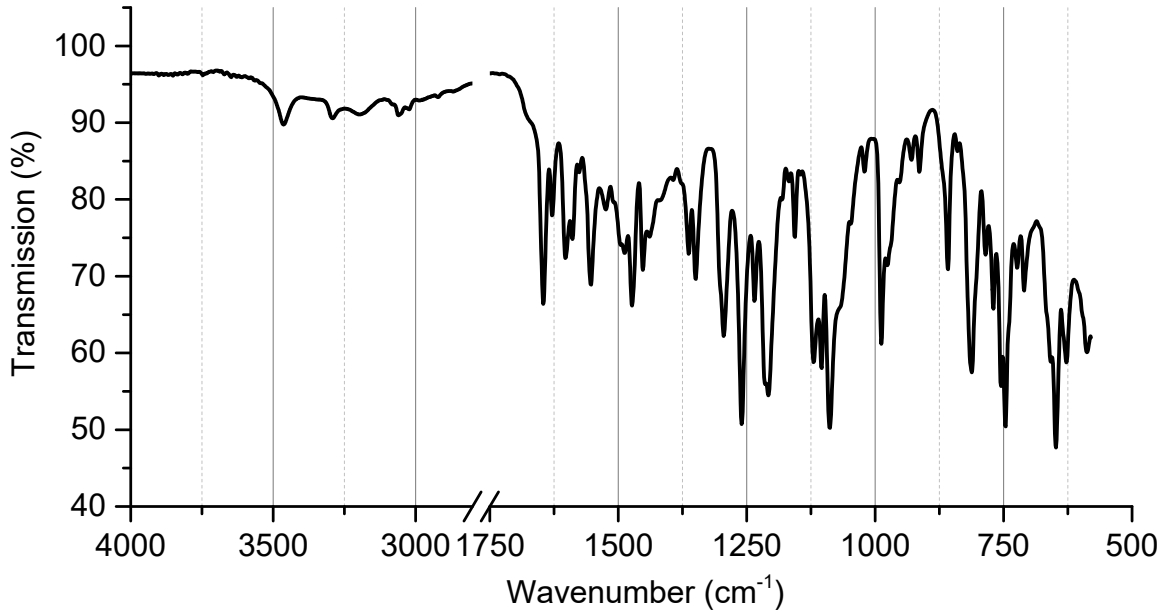

Fig. S 9 IR spectrum of $K(H_2O)_n[Yb(L^2)_2]$

TGA data

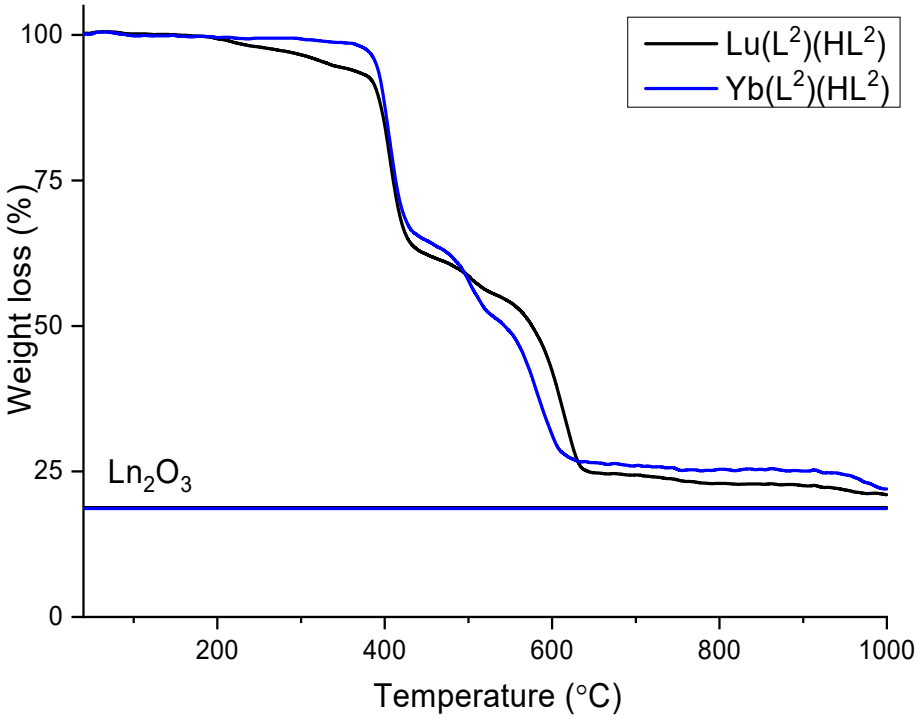

Fig. S 10 TGA data of $Lu(L^2)(HL^2)$, $Yb(L^2)(HL^2)$

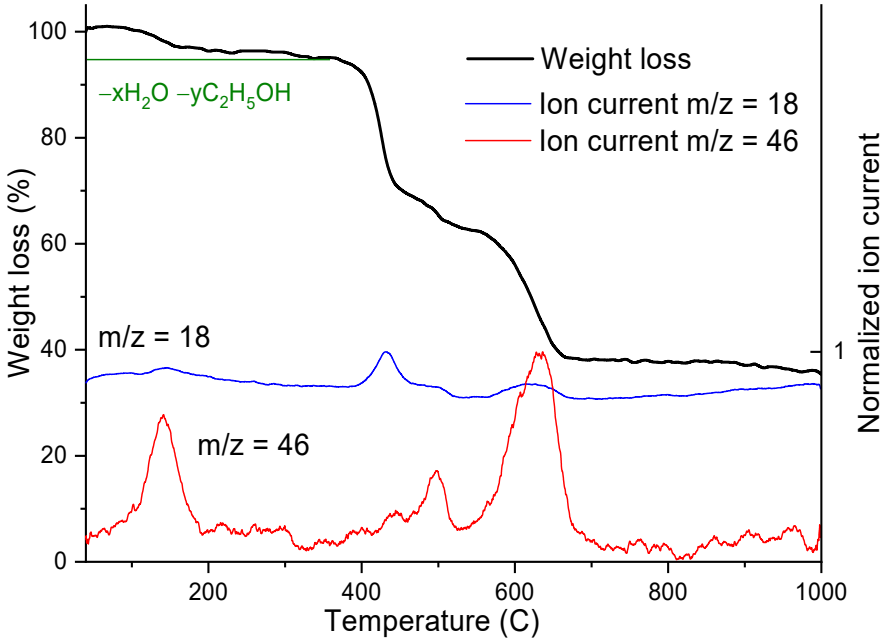

Fig. S 11 TGA data of $K(H_2O)_x(EtOH)_y[Yb(L^2)_2]$

Photophysical data

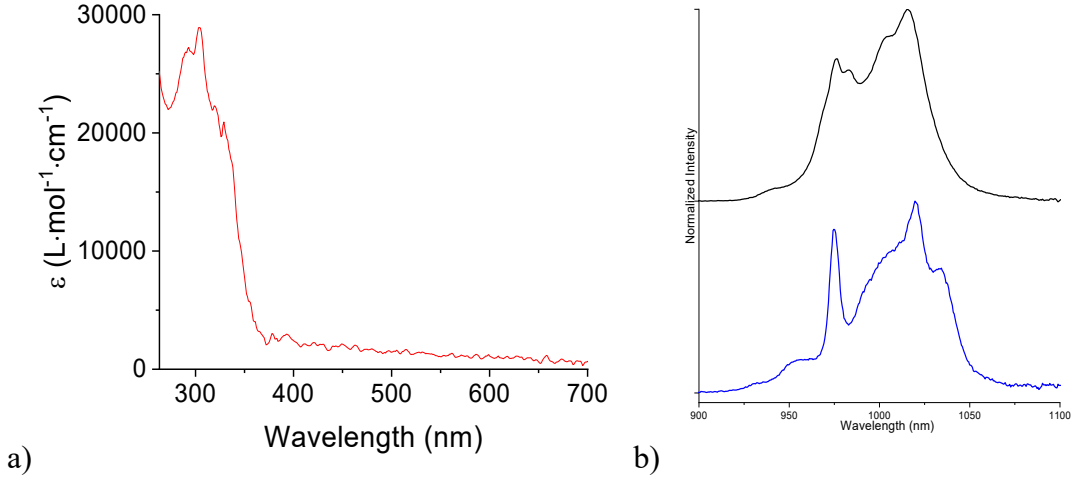

Fig. S 12 a) H_2L^2 absorption spectrum (acetonitrile, 10^{-5} M), b) emission spectra of $Yb(L^2)(HL^2)$ (up) and $K(H_2O)_2(EtOH)[Yb(L^2)_2]$ (down) at RT.

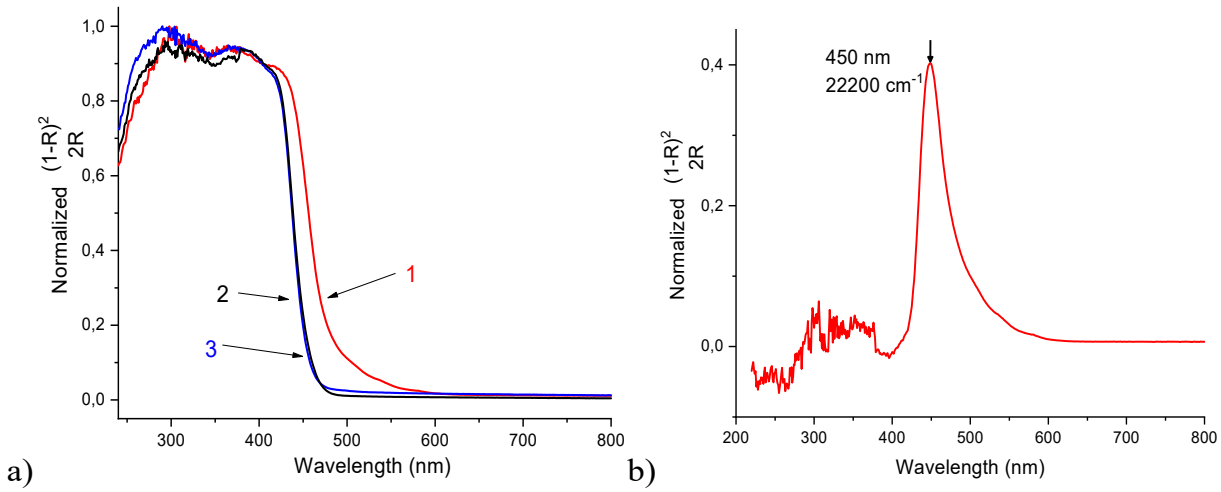

Fig. S 13 a) DR spectra of $Lu(L^2)(HL^2)$ (Ln = Eu (1, red), Yb (3, blue), and Lu (2, black)) and b) the difference between DRS of $Lu(L^2)(HL^2)$ (Ln = Eu, Lu).

The diffuse reflectance (DR) spectra (Figure S13) were obtained to determine the presence of the ligand to metal charge transfer state (LMCT) in europium complex (in which the LMCT state can exist) by comparing its DR spectra with that of the lutetium complex (in which the LMCT state can not exist). In the DR spectrum of $Eu(L^2)(HL^2)$, the red absorption edge is at longer wavelengths than for the $Lu(L^2)(HL^2)$; subtraction of the $Lu(L^2)(HL^2)$ spectrum from the $Eu(L^2)(HL^2)$ spectrum results in an intense band with a maximum at 470 nm (22200 cm^{-1}) corresponding to the LMCT band.

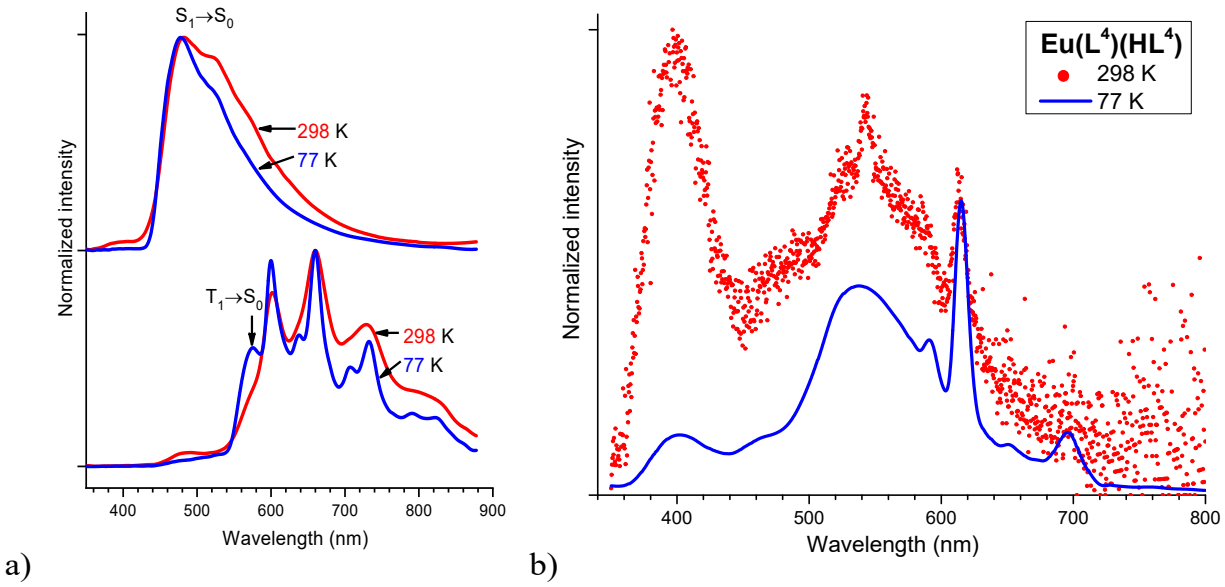

Fig. S 14 a) PL spectra of $Ln(L^2)(HL^2)$ (Ln = Lu (above), Gd (below)) at RT (red) and 77K (blue). b) PL spectra of $Eu(L^2)(HL^2)$ at RT (red) and 77K (blue)

Triplet state energy calculation

To calculate the triplet state energies, the typical approach to record the low-temperature luminescence of the gadolinium was used; in addition lutetium complex luminescence was also studied.[4] As expected, $Lu(L^2)(HL^2)$ demonstrated only a broadband fluorescence at both room and low temperature, which FWHM decrease upon cooling down to 77K (liquid nitrogen). Unlike diamagnetic lutetium, paramagnetic gadolinium tends to enhance ligand phosphorescence in its complexes.[5] Indeed, a red-shifted luminescence, corresponding to ligand phosphorescence, was observed for $Gd(L^2)(HL^2)$ at both temperatures. At room temperature, an additional low-intensity fluorescence band was also observed at ca. 490 nm, which disappeared upon cooling, in parallel with the phosphorescent bands narrowing.

The triplet state energy was calculated from the position of the 0-0 phonon band of the $Gd(L^2)(HL^2)$ spectrum at low temperature, while to estimate the S_1 energy, the maximum of the $Lu(L^2)(HL^2)$ luminescence band was used.

Verification of the concentration quenching

Complexes $(Yb_xLu_{1-x})(L^1)(HL^1)$ (x = 0.1 and 0.5) were obtained from $(Yb_xLu_{1-x})(OH)_3$, freshly prepared from solution, containing $Yb_xLu_{1-x}Cl_3{\cdot}6H_2O \equiv xYbCl_3{\cdot}6H_2O$ and (1-x) $LuCl_3{\cdot}6H_2O$

according to reaction (1), similarly to described in ref [6]. Analysis of their luminescent properties revealed that neither luminescence lifetime, nor quantum yield changed upon the partial substitution of Yb ion with Lu, indicating the unexpected absence of the concentration quenching. This means that due to the mononuclear structure of the $Yb(L^1)(HL^1)$ molecule the metal-to-metal distance is large enough to prevent Yb-Yb interaction, resulting in the absence of concentration quenching. Since larger Yb…Yb distance is expected in complexes with L^2 due to the presence of a larger substituent, concentration quenching is not expected for them as well.

Quantum calculations

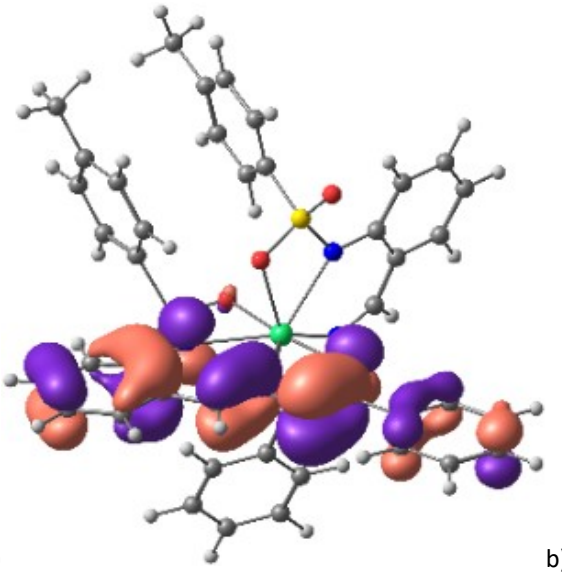

a)

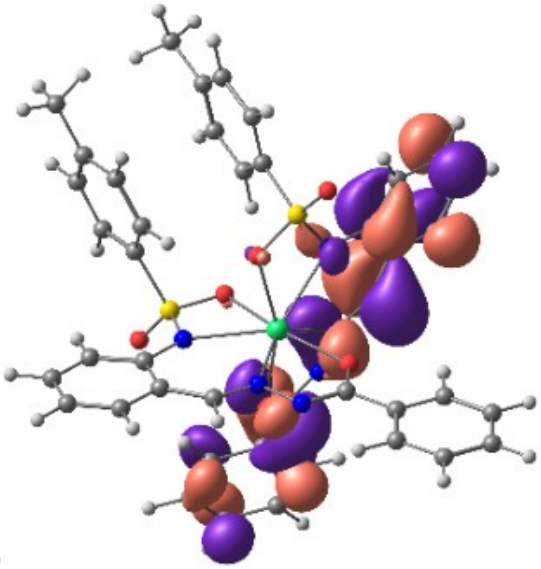

b)

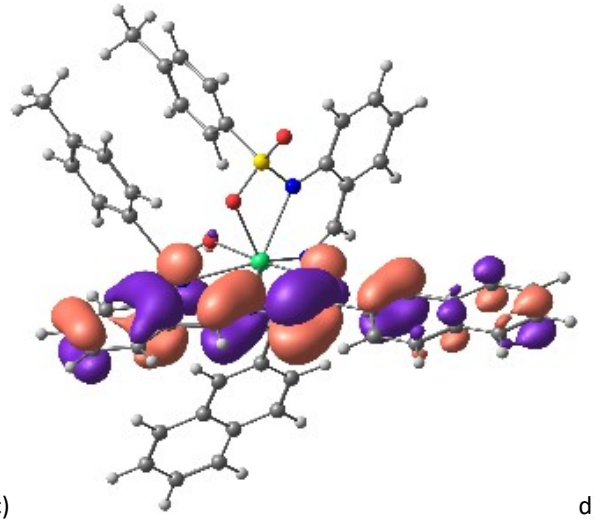

c)

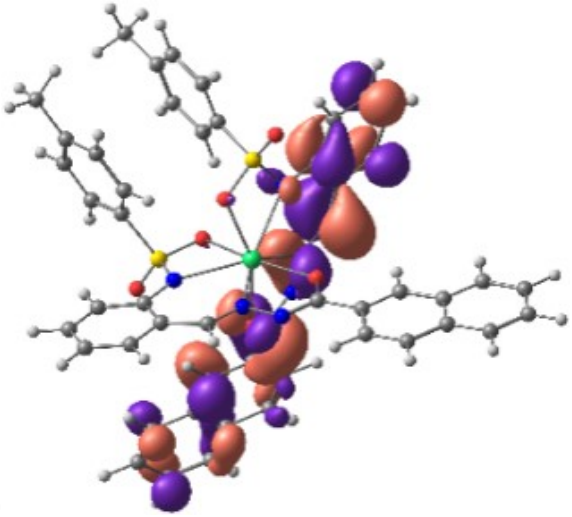

d)

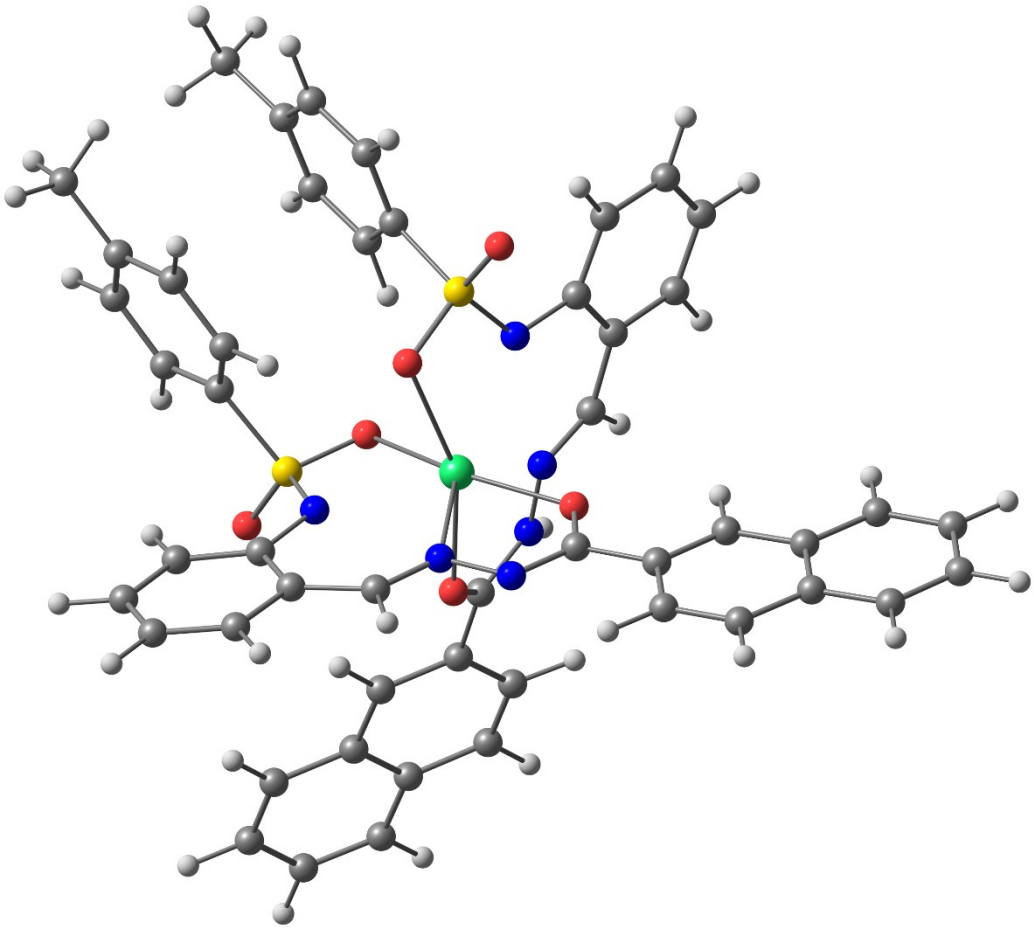

e)

Fig. S 15 Localization of a,c) HOMOs and b,d) LUMOs in a,b) Yb(L^1)(HL^1) and c,d) Yb(L^2)(HL^2). e) Optimized ground state geometry of Yb(L^2)(HL^2).